Intercell Interference Coordination for UAV Enabled URLLC With Perfect/Imperfect CSI Using Cognitive Radio

ALI RANJHA [1], MUHAMMAD AWAIS JAVED [2], GAUTAM SRIVASTAVA (Senior Member, IEEE)[3,4,6], AND JERRY CHUN-WEI LIN [5] (Senior Member, IEEE)

[1]Department of Electrical Engineering, École de Technologie Supérieure, Montréal, QC H3C 1K3, Canada

[2]Department of Electrical and Computer Engineering, COMSATS University Islamabad, Islamabad 45550, Pakistan

[3]Department of Math and Computer Science, Brandon University, Brandon, MB R7A 6A9, Canada

[4]Research Centre for Interneural Computing, China Medical University, Taichung 404, Taiwan

[5]Department of Computer Science, Electrical Engineering and Mathematical Sciences, Western Norway University of Applied Sciences, 5020 Bergen, Norway

[6]Department of Computer Science and Math, Lebanese American University, Beirut 1102, Lebanon

CORRESPONDING AUTHOR: J. C.-W. LIN (e-mail: jerrylin@ieee.org)

This work was supported in part by the Western Norway University of Applied Sciences, Bergen, Norway.

ABSTRACT Ultra-reliable and low latency communications (URLLC) will be the backbone of the upcoming sixth-generation (6G) systems and will facilitate mission-critical scenarios. A design accounting for stringent reliability and latency requirements for URLLC systems poses a challenge for both industry and academia. Recently, unmanned aerial vehicles (UAV) have emerged as a potential candidate to support communications in futuristic wireless systems due to providing favourable channel gains thanks to Line-of-Sight (LoS) communications. However, usage of UAV in cellular infrastructure increases interference in aerial and terrestrial user equipment (UE) limiting the performance gain of UAV-assisted cellular systems. To resolve these issues, we propose low-complexity algorithms for intercell interference coordination (ICIC) using cognitive radio when single and multi-UAVs are deployed in a cellular environment to facilitate URLLC services. Moreover, we model BS-to-UAV (B2U) interference in downlink communication, whereas in uplink we model UAV-to-BS (U2B), UAV-to-UAV (U2U), and UE-to-UAV (UE2U) interference under perfect/imperfect channel state information (CSI). Results demonstrate that the proposed perfect ICIC accounts for fairness among UAV especially in downlink communications compared to conventional ICIC algorithms. Furthermore, in general, the proposed UAV-sensing assisted ICIC and perfect ICIC algorithms yield better performance when compared to conventional ICIC for both uplink and downlink for the single and multi-UAV frameworks.

INDEX TERMS URLLC, multi-UAV, cognitive radio, intercell interference coordination (ICIC).

I. INTRODUCTION

ULTRA-RELIABLE and low-latency communications are one of the key services which is present in the current fifth-generation (5G) as well as futuristic sixth-generation (6G) networks [1], [2], [3], [4].

Comparably, 5G Ultra-reliable and low latency communications (URLLC) cannot satisfy all the key performance indicators (KPIs) of wide and diverse mission-critical applications such as virtual/augmented reality (VR/AR), Industry 5.0, Meta-Universe, unmanned aerial vehicles (UAVs) control, non-payload communications (CNPC), tactile Internet, etc. [5], [6], [7], [8], [9], [10], [11], [12]. As such, to provide adequate services to these applications, 6G networks are envisioned to satisfy additional KPIs integrated with URLLC such as high energy efficiency, spectrum utility, network availability, ultra-high reliability, as well as low latency and

the round-trip delay. Moreover, depending on the mission-critical application at hand, the ultra-high reliability target can drop to a lower value, i.e., 10^{-9}, as such, 5G networks are not designed to cater to such stringent reliability targets for facilitating URLLC services [13]. Under such conditions, 6G networks come to the rescue and aim to enhance URLLC services by improving both fronts, namely reliability and latency targets by at least two magnitude folds. Presently, for radio access networks (RAN), 5G networks can realistically achieve the target of 1 ms transmission delay [14], [15], [16], [17]. Nonetheless, transmission delay amounts to a small portion of end-to-end (E2E) delay, whereas other delay types such as processing, queuing, round trip hybrid automatic repeat request (HARQ), and packet decoding delays also factor in and contribute significantly to the overall E2E delay, which in turn could deter URLLC targets by becoming bottlenecks in networks. Additionally, latency and reliability are present on the opposite end of the same spectrum, i.e., they are inversely proportional [18]. Therefore, these relevant issues about latency and reliability have not been properly investigated by present 5G networks. Moreover, URLLC systems generate short blocklength packets which follow the so-called *finite blocklength capacity formula*. As such, URLLC systems are not throughput-centric but are latency and reliability centric which signals a shift in paradigm from previous wireless communication technologies. Thus, for finite blocklength, URLLC packets, the capacity bounds, and channel coding rates were derived and reviewed in [19].

In recent years, Unmanned Aerial Vehicles (UAV) have become more prominent and are used in public, military, and industrial applications. In this regard, a report from the Federal Aviation Administration (FAA) mentions that the fleet of drones will be almost doubled from 1.1 million units in 2017 to 2.4 million units by the year 2022 [20]. Moreover, UAV-enabled communications have appeared as a prevalent choice due to providing favourable channel gains thanks to line of sight (LoS) communications. Additionally, UAV can act as an aerial base station (ABS) and flying relays to facilitate communications as outlined in [21], [22], [23], [24], [25], [26], [27]. In [21], the authors studied a novel UAV trajectory design based on the so-called *finite Fourier series* (FFS) for multiple ground users. The authors aimed to optimize the max-min rate for all the users. Moreover, the authors demonstrated that their proposed approach yielded superior performance compared to the baseline scheme designed using discrete waypoints. In [22], the authors consider both the average packet error probability (APEP) as well as effective throughput (ET) of the control link in UAV communications, where the ground users are sending control signals to the UAV requiring URLLC. In this regard, the authors derived the closed-form expressions for both APEP and ET by making use of the so-called Gaussian-Chebyshev quadrature and then verified the analytical results by performing Monte-Carlo simulations. Similarly, in [23], the authors considered UAV as an ABS serving multiple ground users. The authors proposed a novel cyclical multiple

access (CMA) to facilitate UAV-to-ground user communication scheduling. Furthermore, the authors sought to optimize the max-min rate between UAV and ground users. In [24], the authors proposed an energy-efficient UAV-relaying scheme to facilitate communication between Base Stations (BS) and ground users. The authors sought to optimize UAV and BS transmit power as well as speed, acceleration, and UAV trajectory to maximize energy efficiency. However, in [21], [22], [23], [24] the interference is overlooked. According to [28], studies have been conducted by the 3rd Generation Partnership Project (3GPP), which highlights the disadvantage of utilizing a UAV in a cellular infrastructure as it could lead to increased interference in a system containing both aerial and ground user equipment (UE) [29]. Thus, only relying on UAV Line of Sight (LoS) links without considering interference will not attain the visionary goal of large-scale UAV deployment in cellular infrastructure for futuristic wireless communication systems. A few works in open technical literature as outlined in [30], [31], have discussed intercell interference coordination (ICIC) techniques in cellular environments to mitigate the adverse effects of interference when UAV are deployed. In [30], the authors considered two user interference channels for the two UAV servicing them. The authors optimized the UAV positioning and transmit power to maximize the sum throughput. However, the authors considered LoS channels for only two users which give limited insights. Similarly, in [31], the authors studied ICIC in cellular-connected UAV using a cognitive radio approach. Nonetheless, the authors did not generalize to a multi-UAV framework concerning interference between UAV deployed in adjacent cells for uplink and downlink communications.

In this paper, we propose low-complexity algorithms for ICIC using cognitive radio when multi-UAVs are deployed in a cellular environment to facilitate URLLC services. Moreover, we model BS-to-UAV (B2U) interference in downlink communication, while in the uplink we model UAV-to-BS (U2B), UAV-to-UAV (U2U), and UE-to-UAV (UE2U) interference under perfect/imperfect channel state information (CSI). Our results show that our proposed perfect ICIC compared to conventional ICIC models fairness among single and multi-UAVs in downlink communications. Moreover, both UAV-sensing assisted ICIC and perfect ICIC algorithms perform better than conventional ICIC for uplink and downlink communications for the proposed single and multi-UAV framework.

A. ORGANIZATION AND NOMENCLATURE
The rest of this paper is organized as follows. In Section II, we present the system model and formulate the problem in the context of UAV-assisted cellular systems. Then, in Section III, we propose our algorithms for single UAV and multi-UAV interference cases, respectively. In Section IV, we present numerical results to verify the proposed algorithm's effectiveness. Finally, we present the conclusion in Section V. The symbols and notations used in this paper are summarized in Table 1.

TABLE 1. Summary of symbols and notations.

| Symbols and notations	Descriptions
$R_{\text{dl, ul}}(n)$	Data rate of each UAV k at each RB n in the uplink and downlink communications
$V(\gamma_{\text{dl, ul}}(k,n))$	Channel dispersion in the the uplink and downlink communications
$I_{\text{dl}}(k,n)$	Interference in the downlink communication
$P_j(n)$	Transmission power of BS j in RB n
$F_j(k,n)$	Downlink channel power gain from BS j to UAV k in RB n
σ^2	Received Gaussian noise power at any UAV
$I_{\text{dl}}(k,n)$	Total Gaussian terrestrial ICI power at UAV k in RB n
$\mathcal{J}(n)$	Set of BSs using RB n
$p_{\text{ul}}(k,n)$	Transmission power of UAV k in RB n
$G_j(k,n)$	Uplink channel power gain from UAV k to BS j in RB n
$I_{\text{ul}}(j_k,n)$	Total uplink interference at UAV k's serving BS j_k from all other non-k UAVs in RB n
$\mathcal{N}_{\text{ul}}(k)$	RBs set for the uplink that is allocated to UAV k by its serving BS
P_{dl}	BS peak available power to maximize the UAV's achievable rate in the downlink
Γ_{U}	Defined threshold of the BS receiver noise power σ^2
$E_{\text{ul}}(k,n)$	Sensed uplink transmission at UAV k in RB n
α_{L}	LoS path-loss exponent
$E_j(k,n)$	Channel gain between UAV k and the UE or UAV served by BS j in RB n in the uplink
X_f	Small-scale Ricean fading
f_c^{GHz}	Carrier frequency expressed in GHz
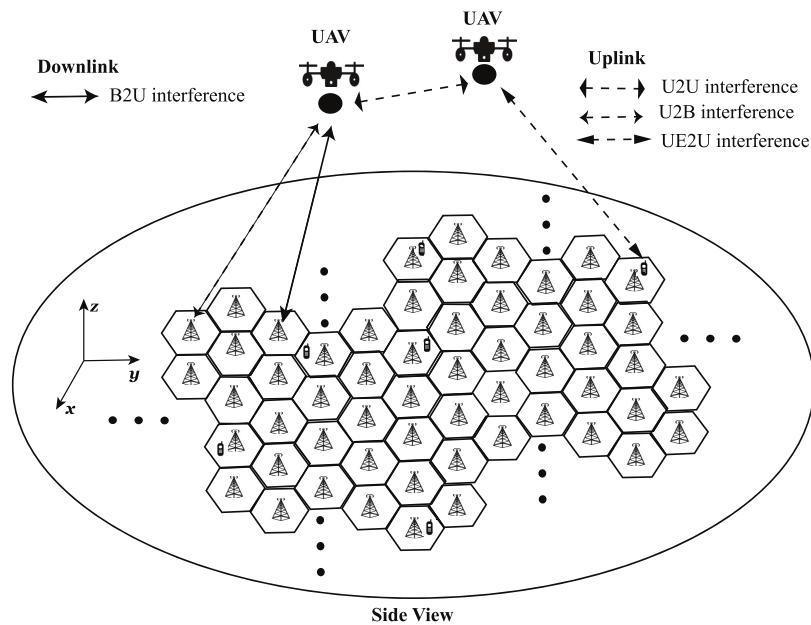
FIGURE 1. Illustration of multi-UAV ICIC for URLLC systems.

II. SYSTEM MODEL AND PROBLEM FORMULATION

We model both downlink and uplink communications facilitated by UAV deployed in hexagonal cells as shown in Fig. 1. Accordingly, a simplistic assumption is made that outside interference is negligible. In our model, BS are primarily placed at the center of each cell with circumradius given by r_c. Additionally, terrestrial UE and UAV are positioned randomly in the given cell environment. As such, each UE and UAV is considered to be assigned to the BS in the cell it is located in or above. Furthermore, each UE gets random resource blocks (RB) assigned such that upon each assignment every previous RB allocation is considered in the following way: there is no resource sharing allowed such that no UE or BS can utilize the same requested RBs in neighbouring cells of nearest q tiers. Equivalently, we can say if q is unity, then no two neighbouring cells can have UE or BS using the same RB. Similarly, if q is two, then we look at two neighbours, i.e., no neighbours of any neighbours of the considered cell may be using the requested RB. Resultantly, strong inter-cell interference (ICI) is mitigated. Additionally, the RB allocation for UAV is performed following the aforementioned neighbour principle relative to its serving BS. It is worth mentioning
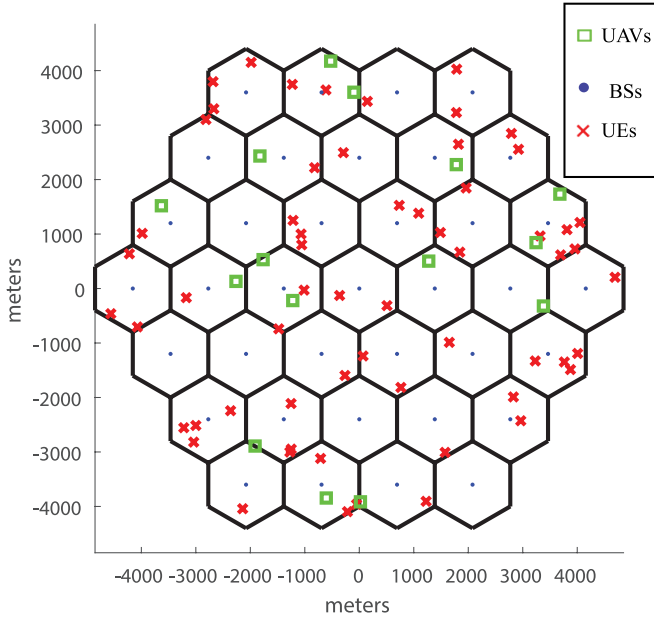
FIGURE 2. Random positioning of UAVs, terrestrial UE, and BSs in the hexagonal cell layout.

that downlink communication is established between BS and UAV, and conversely, uplink communication is established between UAV and BS. According to [32], to calculate the data rate $R_{\text{dl, ul}}(n)$[1] of each UAV k at each RB n in the uplink and downlink communications for short URLLC packets, we use the data rate equation

$$R_{\text{dl, ul}}(k, n) = B \log_2\big(1 + \gamma_{\text{dl, ul}}(k, n)\big) - B \frac{Q^{-1}(\varepsilon)}{\ln 2} \sqrt{\frac{V\big(\gamma_{\text{dl, ul}}(k, n)\big)}{M}}, \tag{1}$$

where $Q^{-1}(\varepsilon) = \sqrt{2}\text{erfc}^{-1}(2\varepsilon)$ is the inverse Q-function, B is the bandwidth, and $V(\gamma_{\text{dl, ul}}(k, n)) = 1 - (1 + \gamma_{\text{dl, ul}}(k, n))^{-2}$ is the channel dispersion, which refers to the channel variability. For the sake of generality, we did not approximate channel dispersion equal to unity as only for high Signal-to-noise ratio (SNR), such an assumption holds, whereas for low SNR it becomes invalid. The second term in (1), is the finite blocklength penalty term. Thereafter, for the downlink communication between BS and UAV, we define interference $I_{\text{dl}}(k, n)$ and SINR $\gamma_{\text{dl}}(k, n)$ as

$$\gamma_{\text{dl}}(k, n) = \frac{P_{j_k}(n) F_{j_k}(k, n)}{\sigma^2 + I_{\text{dl}}(k, n)}, \tag{2}$$

$$I_{\text{dl}}(k, n) = \sum_{i \in \mathcal{J}(n) \setminus \{j_k\}} P_i(n) F_i(k, n), \tag{3}$$

where $P_j(n)$ is the transmission power of BS j in RB n, $F_j(k, n)$ is the downlink channel power gain from BS j to

---

1. For uplink and downlink communications, Shannon's capacity for a user is given by $R_{\text{dl,ul}}(k, n) = B \log_2(1 + \gamma_{\text{dl, ul}}(k, n))$. Comparably, the finite blocklength capacity equation is given by $R_{\text{dl, ul}}(k, n) = B \log_2(1 + \gamma_{\text{dl, ul}}(k, n)) - B \frac{Q^{-1}(\varepsilon)}{\ln 2} \sqrt{\frac{V(\gamma_{\text{dl, ul}}(k, n))}{M}}$. Furthermore, the additional terms are the penalty terms incurred due to short blocklengths. Therefore, for the large blocklengths, i.e., approaching infinity, the penalty terms cease to exist, and the finite blocklength capacity simply reduces to Shannon's capacity.

UAV k in RB n, j_k denotes the BS serving UAV k, and σ^2 is the received Gaussian noise power at any UAV. Moreover, $I_{\text{dl}}(k, n)$ is the total Gaussian terrestrial ICI power at UAV k in RB n, $\mathcal{J}(n)$ is the set of BSs using RB n. Now, for a multi-UAV environment, we define $\mathcal{J}(n)$, which requires subtraction of sets $\mathcal{J}(n) \setminus \{j_k\}$ when used as a set of indices. Now, for the uplink communication between the UAV and the BS, we model SINR $\gamma_{\text{ul}}(k, n)$ as

$$\gamma_{\text{ul}}(k, n) = \frac{p_{\text{ul}}(k, n) G_{j_k}(k, n)}{\sigma^2 + I_{\text{ul}}(j_k, n)}, \tag{4}$$

$$I_{\text{ul}}(j_k, n) = \sum_{l \in \mathcal{K}(n) \setminus \{k\}} p_{\text{ul}}(l, n) G_{j_k}(l, n), \tag{5}$$

where $p_{\text{ul}}(k, n)$ is the transmission power of UAV k in RB n, $G_j(k, n)$ is the uplink channel power gain from UAV k to BS j in RB n, and σ^2 is the Gaussian noise power at the receiver of any BS. Moreover, $I_{\text{ul}}(j_k, n)$ denotes the total uplink interference at UAV k's serving BS j_k from all other non-k UAVs in RB n. Additionally, another important interference is the maximum interference UAV k causes to any other non-j_k BS using the same RBs, which is given as

$$I_{\text{ul}}(k) = \max_{n \in \mathcal{N}_{\text{ul}}(k), \; j \in \mathcal{J}(n) \setminus \{j_k\}} p_{\text{ul}}(k, n) G_j(k, n), \tag{6}$$

where $\mathcal{N}_{\text{ul}}(k)$ denotes the RBs set for the uplink that is allocated to UAV k by its serving BS. Conversely, $\mathcal{N}_{\text{dl}}(k)$ denotes the RBs set for the downlink, respectively. In both the conventional and UAV-sensing-assisted ICIC for the downlink, the power control is simple: BS always use peak available power P_{dl} to maximize the UAV's achievable rate in the downlink. Similarly, in the conventional ICIC in the uplink peak power P_{ul} is always used. However, in the uplink in the UAV-sensing-assisted model outlined in [31], the power control is more complicated. Here, we generalize it to the kth UAV as

$$p_{\text{ul}}(k, n) = \min \left\{ 1, \frac{\Gamma_{\text{U}} \rho_k^{\alpha_{\text{L}}}}{E_{\text{ul}}(k, n)} \right\} P_{\text{ul}}, \tag{7}$$

where Γ_{U} is a defined threshold of the BS receiver noise power σ^2, $E_{\text{ul}}(k, n)$ is the sensed uplink transmission at UAV k in RB n, α_{L} denotes the LoS path-loss exponent, and ρ_k has a complex expression for distance as outlined in (8) in [31]. Moreover, the main idea behind $E_{\text{ul}}(k, n)$ as described in detail in [31] is that we do not have the knowledge of the CSI, hence we have to predict it from sensed UE uplink transmissions. Thus, the fundamental difference here is that the sensed transmissions will also include transmissions from other UAV. This will result in a higher $E_{\text{ul}}(k, n)$ and hence a lower $p_{\text{ul}}(k, n)$ than in [31]. The formulation is given as

$$E_{\text{ul}}(k, n) = P_{\text{ul}} \sum_{j \in \mathcal{J}(n)} E_j(k, n), \tag{8}$$

where $E_j(k, n)$ is the channel gain between UAV k and the UE or UAV served by BS j in RB n in the uplink. Moreover,

if we know the CSI, the power allocation would simply use the known $G_j(k, n)$ as

$$p_{ul}^*(k, n) = \min\left\{\min_{j \in \mathcal{J}(n)} \frac{\Gamma_U}{G_j(k, n)}, P_{ul}\right\}. \quad (9)$$

Finally, achievable rates $R_{dl}(k, n)$ or $R_{ul}(k, n)$ for both uplink or downlink communications are given by replacing Signal-to-interference-plus-noise ratio (SINR) given by (2) or (4) in (1). Therefore, the total sum achievable rates over the used RB are given by

$$R_{T\ dl,\,ul}(k) = \sum_{n \in \mathcal{N}_{dl,\,ul}(k)} R_{dl,\,ul}(k, n). \quad (10)$$

According to [31], for all channel gains the probabilistic 3GPP Urban Macro path loss model is the suitable choice. Additionally, with our given simulation parameters, a UAV altitude of at least 200 metre (m) gives us a pure LoS model, to which we add small-scale Ricean fading denoted by X_f, thus we have

$$PL(d) = 28 + 22 \log_{10}(d) + 20 \log_{10}\left(f_c^{GHz}\right) + X_f, \quad (11)$$

where f_c^{GHz} is the carrier frequency expressed in GHz. To obtain gain, we negate PL and convert it to linear.

III. PROPOSED ALGORITHMS
In this section, we outline our proposed algorithms for single and multi-UAV interference scenarios.

A. PROPOSED ALGORITHMS FOR SINGLE-UAV INTERFERENCE
We propose three algorithms UAV-enabled common (CMN)-ICIC, UAV-enabled cognitive-sensing based superior (CSS)-ICIC, and UAV-enabled cognitive-sensing based (CSB)-ICIC. **Algorithm 1** outlines UAV-enabled CSS-ICIC, which is repeated over random initializations L_{in} times, then all the results are averaged over L_{avg} iterations. Furthermore, for **Algorithm 1**, the UAV-enabled CMN-ICIC would omit **step 9** and determine $\mathcal{N}_{dl,\,ul}$ by simply assigning the UAV random RB with neighbor criterion in mind, and by setting $p_{ul}(n) = P_{ul}\ \forall n$. Additionally, M_d denotes the number of RB candidates in the downlink, and UAV-enabled CSB-ICIC sets M_d to the number of available RBs after UE RB allocation. In other words, UAV-enabled CSB-ICIC is equivalent to UAV-enabled CMN-ICIC if we set M_d or M_u equal to the number of available RBs after UE RB allocation. Hence, **Algorithm 1** represents all the proposed algorithms with a few changes. Additionally, for the proposed schemes, including UAV-enabled CMN-ICIC, CSS-ICIC, and CSB-ICIC for the downlink, the power control is simple: the BSs always use peak available power P_{dl} to maximize the UAV's achievable rate. Similarly, for the UAV-enabled CMN-ICIC, in the uplink, peak power P_{ul} is always used. Conversely, UAV-enabled CSS-ICIC and CSB-ICIC both utilize (6) for power control in uplink communications to maximize the UE's data rate. To determine the sum complexity, we note

---

Algorithm 1 UAV-Enabled CSS-ICIC

1: **Set:** M_d or M_u to be the number of RB candidates the UAV considers for UAV-enabled CSS-ICIC.
2: **Set:** N_d or N_u to be the number of RBs the UAV requests for UAV-enabled CMN-ICIC.
3: **Set:** r_c to be the cell circumradius.
4: **Set:** q to be the number of tiers for the neighbor criterion.
5: **Initialize:** A network of adjacent hexagonal cells with a BS in the center of each cell.
6: **Initialize:** Random UAV's placement in cell 1 (central cell) and all UEs placement randomly within the whole cell-covered territory.
7: **Initialize:** Random assignment of RBs to each UE s.t. $\forall e_1 \in$ {UEs} $\forall e_2 \in$ {UEs} $(e_2 \in N_{e_1}(q)) \Rightarrow (RB(e_1) \neq RB(e_2))$ where $N_{e_1}(q) = $ {UEs within q tiers away from UE e_1}.
8: **Define:** $\mathcal{J}(n) = $ {BS using RB n}.
9: **Calculate:** A requested amount of RB candidates (or as many as possible if the requested amount is unavailable) is chosen randomly to be assigned to the UAV, but also such that no UEs or equivalently BSs within the nearest q tiers are using it.
10: **for** each RB candidate **do**
11:     **Calculate:** $F_i(n)$ or $G_i(n)\ \forall i \in \mathcal{J}(n) \cup \{1\}$ using (11).
12:     **Calculate:** $\gamma_{dl}(n)$ using (2), and $I_{dl}(n)$ using (3), for the downlink.
13:     **Calculate:** $p_{ul}(n)$ using (7), and $\gamma_{ul}(n)$ using (4), for the uplink.
14:     **Calculate:** $R_{dl,\,ul}(n)$ using (1).
15: **end for**
16: **Calculate:** $\mathcal{N}_{dl,\,ul} = $ {Highest N_d or N_u RB ranked by value of $R_{dl,\,ul}(n)$}.
17: **Return:** $R_{T\ dl,\,ul}$ using (10) or I_{ul} using (6) for the uplink.

---

that all steps after the **for** loop are constant-time. The step preceding the **for** loop takes at most $O(N_{rb})$ time, where N_{rb} is the number of RB because at worst the algorithm has to look through all N_{rb} RB before coming up with enough candidates. Thus, the **for** loop deterministically cycles through all M_d/M_u candidates in the downlink/uplink. Consequently, the total time complexity for the UAV-enabled CSS-ICIC is $O(N_{rb}) + O(M_d) + O(1)$. Therefore, the total time complexity is $O(L_{it}N_{rb})$, where L_{it} is the number of iterations in the **for** loop in **Algorithm 1**, for both downlink and uplink with the UAV-enabled CSS-ICIC. Similarly, for the UAV-enabled CMN-ICIC, the **for** loop cycles through N_d or N_u elements, while the time complexity of the other parts remains the same. Hence, $O(L_{it}N_{rb})$ remains the dominant term. Therefore, specifically about the algorithms' programming, $O(L_{it}N_{rb})$ is the time complexity for both UAV-enabled CMN-ICIC and CSS-ICIC in both downlink and uplink. Since the UAV-enabled CSB-ICIC is equivalent to the UAV-enabled CMN-ICIC with maximum M_d or M_u, hence it yields a similar time complexity. However, since a higher number of candidates means more iterations in the **for** loop, this translates to more calculation time and energy expenditure by the UAV. In this regard, we could optimize the time complexity of the UAV-enabled CSB-ICIC using vectorization of loops, which moderately increases the memory resources. Nevertheless, this is not an issue for modern UAVs equipped with a powerful system of chips (SoC).

Algorithm 2 UAV-Sensing Assisted ICIC for Multi-UAVs

1: **Set:** q to be the number of tiers for the neighbor criterion.
2: **Set:** M_d or M_u to be the number of RB candidates the UAV considers.
3: **Set:** N_d or N_u to be the number of RBs the UAV requests.
4: **Choose:** M_d or M_u RB candidates (or as many as possible if the requested amount is unavailable) are chosen randomly to be assigned to the UAV, but also such that no BSs within the nearest q tiers of the UAV's serving BS is using it.
5: **for** each RB candidate **do**
6:    **Sense:** Interferences $I_{dl}(k, n)$ for downlink or $E_{ul}(k, n)$ for uplink are sensed by the UAV in each candidate RB n.
7:    **Return:** $\mathcal{N}_{dl,\,ul} = \{$best N_d or N_u RBs ranked by lowest sensed interference$\}$.
8:    **Return:** If in uplink, calculate power control by (7).
9: **end for**

B. PROPOSED ALGORITHMS FOR MULTI-UAV INTERFERENCE CASE

For the conventional ICIC, a requested number of RB is simply assigned randomly. However, in the UAV-sensing-assisted ICIC proposed in [31], a more complex algorithm is at play wherein a given number of candidates are first randomly picked out complying with the neighbor requirement, of which those with the lowest sensed interference are chosen to be assigned to the UAV. Now, we outline the UAV-sensing assisted ICIC scheme for multi-UAV framework, whereas the conventional ICIC would eliminate the entire candidates part and determine $\mathcal{N}_{dl,\,ul}(k)$ by simply assigning the UAV random RB with neighborhood criterion, and by setting $p_{ul}(k, n) = P_{ul}$, $\forall k \forall n$. Further, M_d or M_u denotes the number of RB candidates in the downlink/uplink, and a perfect ICIC takes M_d or M_u equal to the total number of RBs in the downlink/uplink. Moreover, N_d or N_u is the number of RBs the UAV requests. Additionally, UAVs become operational one after another, and RB allocation for each UAV is to be done only upon it becomes operational in the service area. This avoids an endlessly iterative process where UAVs would constantly be changing their allocation to account for changes in the environment. Here, **Algorithm 2**, outlines the program executed in each UAV, whereas **Algorithm 3**, outlines the scheme we use to simulate the whole environment and extract real data rates and interferences.

Now we determine the time complexity of the ICIC **Algorithm 2**, implemented in each UAV. The `for` loop deterministically cycles through all M_d or M_u candidates and performs spectrum sensing. All other steps are constant time. Therefore, the total time complexity for the UAV-sensing ICIC is $O(M_d) + O(1) = O(M_d)$. The conventional ICIC avoids a loop and simply randomly assigns RBs, hence it is constant time.

IV. NUMERICAL RESULTS

For all calculations, we use the setup defined in Table 2.

Algorithm 3 Environment Simulation for Multi UAV-Assisted Cellular Network

---

1: **Set:** r_c to be the cell circumradius.
2: **Set:** q to be the number of tiers for the neighbor criterion.
3: **Initialize:** A network of adjacent hexagonal cells with a BS in the center of each cell.
4: **Initialize:** Randomly placed UAV and UE within the whole cell-covered territory. A UE or UAV is considered to belong to the BS that serves the cell it is in or above.
5: **Initialize:** Random assignment of RBs to each UE s.t. such that no UEs within the nearest q tiers are using it.
6: **Define:** $\mathcal{J}(n) = \{$BSs using RB $n\}$
7: **for** each UAV k **do**
8:    **Run:** Algorithm 2. For sensed interferences use (3) or (8).
9:    **Return:** $R_{T\,dl,\,ul}(k)$ using (10).
10:    **Return (uplink only):** $I_{ul}(k)$ using (6).
11:    **Update:** $\mathcal{J}(n) \leftarrow \mathcal{J}(n) \cup \{j_k\} \, \forall n \in \mathcal{N}_{dl,\,ul}(k)$
12:    **Update (uplink only):** $\mathcal{K}(n) \leftarrow \mathcal{K}(n) \cup \{k\} \, \forall n \in \mathcal{N}_{ul}(k)$
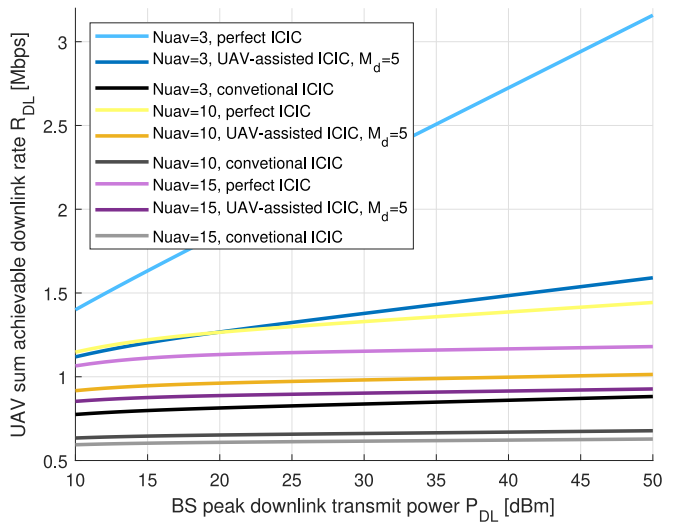13: **end for**

FIGURE 3. UAV sum achievable downlink rate versus BS peak downlink transmit power.

TABLE 2. Simulation parameters.

Parameter	Value
Number of cells with BSs at their centers	37
BS height H_{BS}	25 m
Cell circumradii	$r_c = 800$ m
Blocklength M	200 symbols
Decoding error probability ε	10^{-9}
Number of terrestrial UEs	60
Number of RBs N	30
Bandwidth of each RB	180 KHz

Additionally, there are 3, 10, or 15 UAV with an altitude[2] between 200 and 500 m. In downlink and uplink, the UAV requests 1 and 5 RB, respectively. Furthermore,

---

2. It is also worth mentioning that according to 3GPP release 15, for UAVs flying at a high altitude, i.e., above 100 m, there is a 100% probability of achieving the LoS. Moreover, LoS path-loss will dominate over the other NLoS components. Thus, UAV will associate itself with a BS with the largest LoS channel gain.
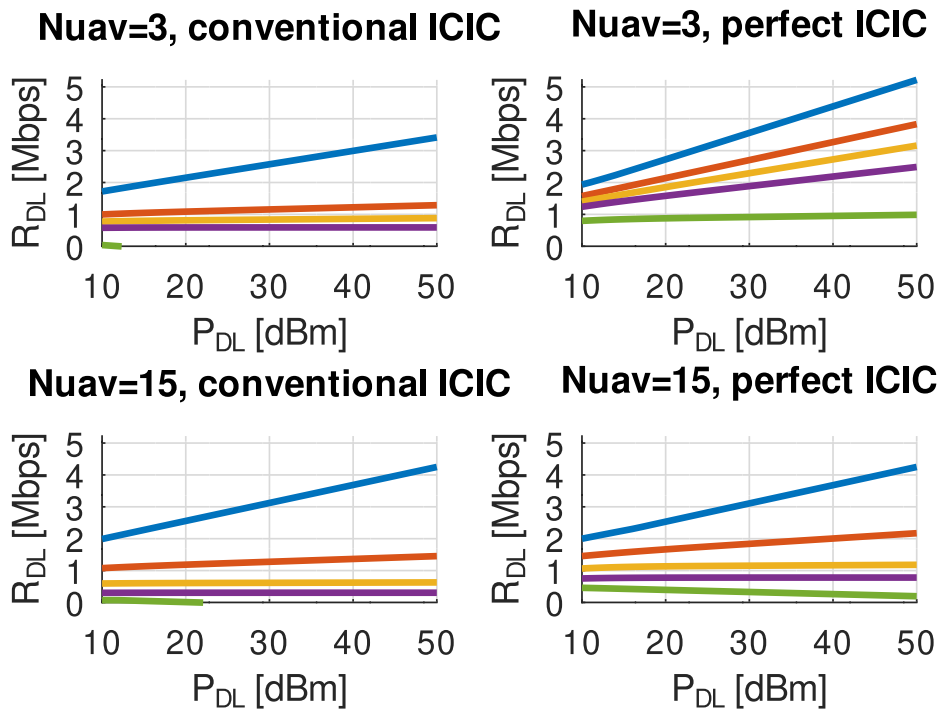
FIGURE 4. UAV sum achievable downlink rate versus BS peak downlink transmit power for fairness among multi-UAVs.
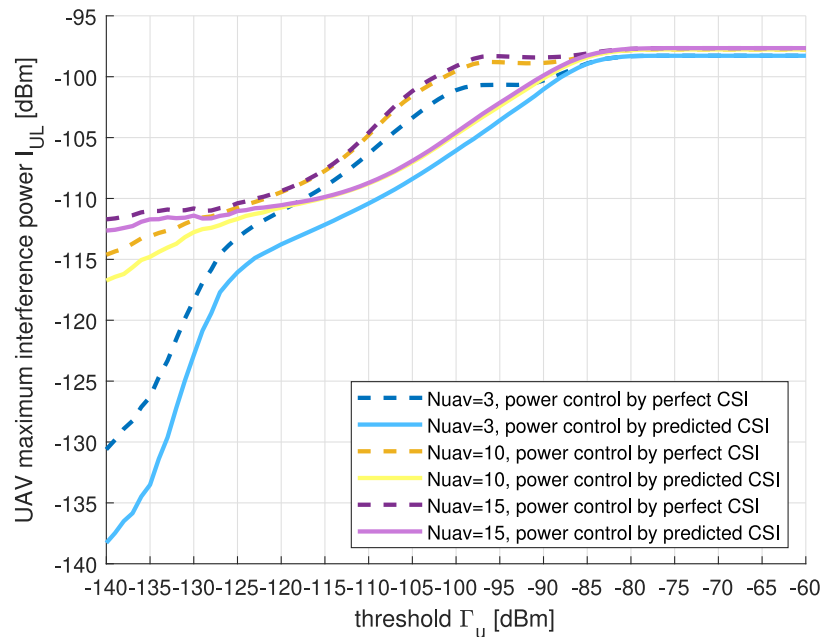

FIGURE 5. UAV maximum interference power versus threshold for uplink power control under perfect/imperfect CSI.

we run 1000 simulations with random channel and location initializations, over which all results are averaged.

A. RESULTS FOR SINGLE UAV INTERFERENCE CASE

In Fig. 7, we demonstrate how the UAV sum uplink rate and maximum interference vary when changing the thresholds for the UAV-enabled CSS-ICIC and UAV-enabled CSB-ICIC. Since there is no threshold for UAV-enabled CMN-ICIC,

there is only one point for it in the plot. It is to be noted that on the plot, the slopes on the left side are negative. To further elaborate on this effect, we again plot the UAV sum uplink rate and maximum interference with variable blocklengths M and decoding error probabilities ε. Now, we look at Fig. 8, the left tails of the curves are sloping down. Due to monotonicity, there is a clear trade-off between interference and data rate in the Shannonian equation with
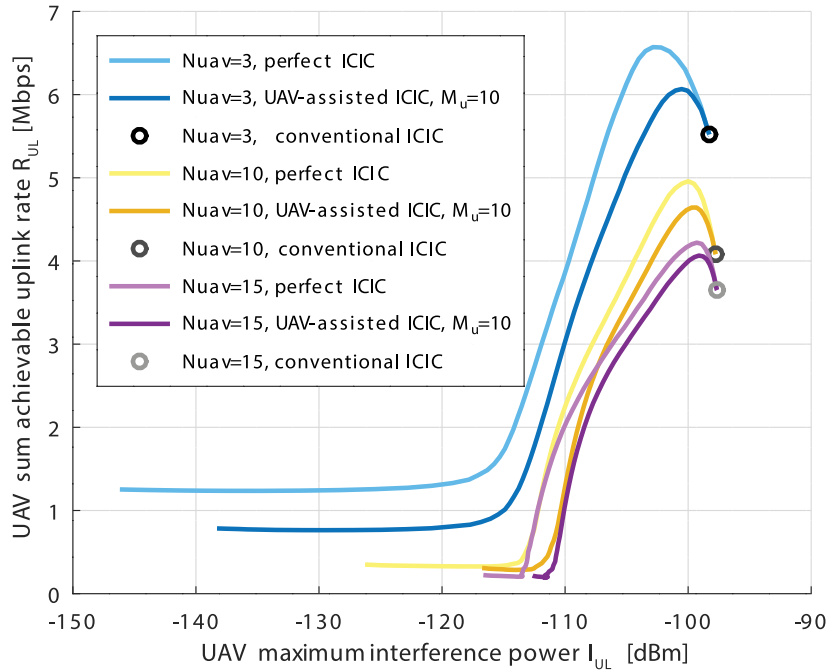
FIGURE 6. UAV sum achievable uplink rate versus UAV maximum interference power.
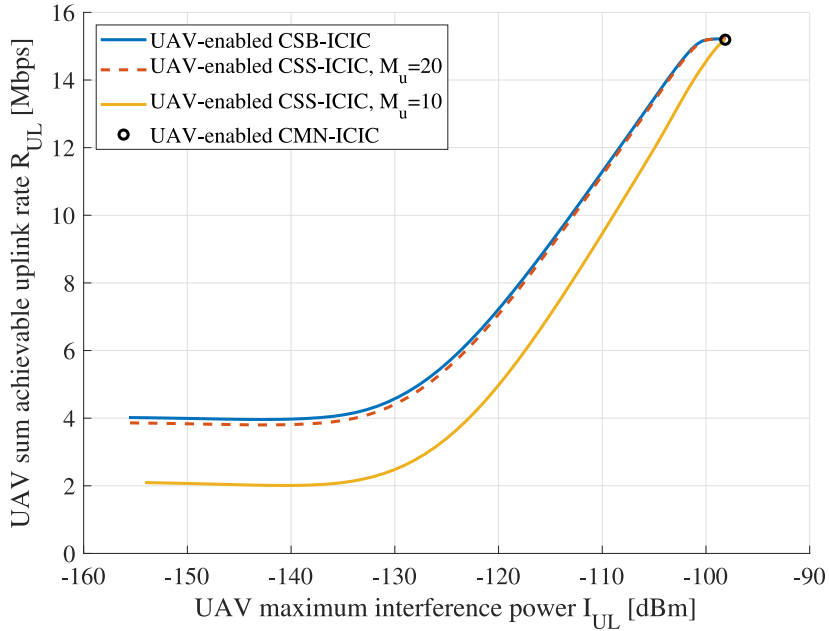

FIGURE 7. UAV sum achievable rate versus maximum interference power in the uplink.

short blocklength data rate due to non-monotonicity; such a trade-off does not necessarily exist. Consequently, we do not have to sacrifice one for the other if we happen to also want to constrain ourselves below a certain interference level, e.g., if we are required to keep interference below -140 dBm which is achieved by appropriately adjusting the threshold Γ_U, then we can simply choose the leftmost point on the curve and be assured that we will both decrease the interference and maximize the data rate under our constraint $I_{ul} \leq -140$ dBm. This is a significant advantage

that mitigates the disadvantage implied by the penalty term. In Fig. 9, we present the effect of the blocklength M and decoding error probability ε on the data rate R_{dl}. Here, we fix $M = 200$ symbols (resp. $\varepsilon = 10^{-9}$) and vary ε (resp. M). Moreover, we set $P_{dl} = 10$ dBm and we observe the behavior of Fig. 9, based on Eq. (1), where blocklength M is present in the denominator of the penalty term of the data rate and $Q^{-1}(\varepsilon)$ function which is monotonically decreasing; hence higher values of M and ε tend to yield higher data rates. In Fig. 10, we compare the UAV downlink sum
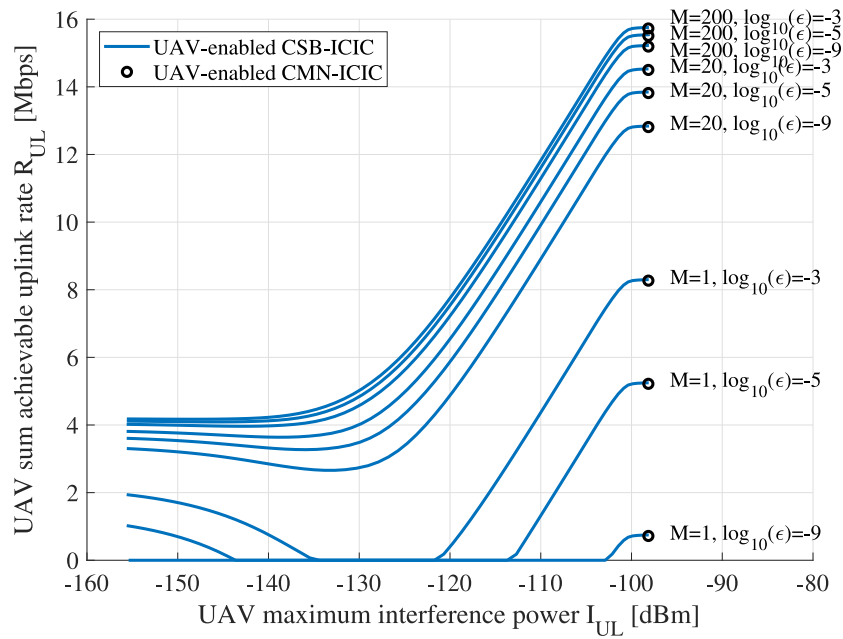
FIGURE 8. UAV sum achievable rate versus maximum interference power in the uplink for variable blocklengths and decoding error probabilities.
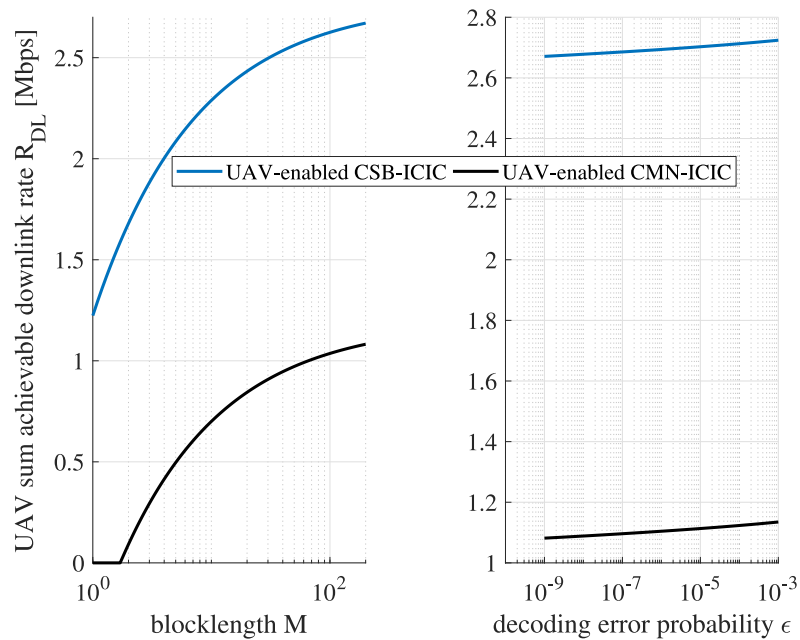

FIGURE 9. UAV sum achievable rate versus blocklength and decoding error probability in the downlink.

achievable data rate R_{dl} to the peak downlink power P_{dl}. Here, we observe that UAV-enabled CSB-ICIC yields the best performance while UAV-enabled CMN-ICIC shows the worst performance. Moreover, we also observe that UAV-enabled CSS-ICIC yields a mediocre performance. However, as M_d increases, its performance becomes superior to that of UAV-enabled CMN-ICIC. Finally, in Fig. 11, we study how the peak power P_{dl} of the BS is adjusted according to the blocklength and decoding error probability. For reference, we use $P_{dl} = 30$ dBm. The graphs in Fig. 11 tell us that

to recover from the lower data rates at lower M and ε, we must increase the power. Resultantly, UAV-enabled CMN-ICIC should adjust its power much more since the slope of its graph in Fig. 10 is much shallower than that of UAV-enabled CSB-ICIC. As evidenced by Fig. 11, the performance of UAV-enabled CSB-ICIC is better than UAV-enabled CMN-ICIC, especially when smaller blocklengths are considered and a lower decoding error probability is required, which is the case for URLLC. Therefore, we recommend the UAV-enabled CSB-ICIC for URLLC systems as it yields the best
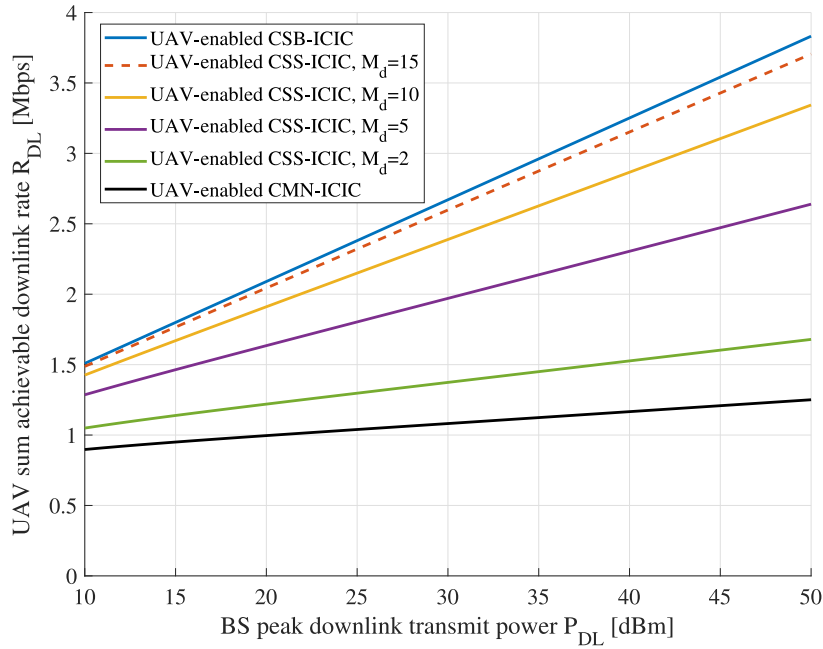
FIGURE 10. UAV sum achievable rate versus BS peak transmit power in the downlink.
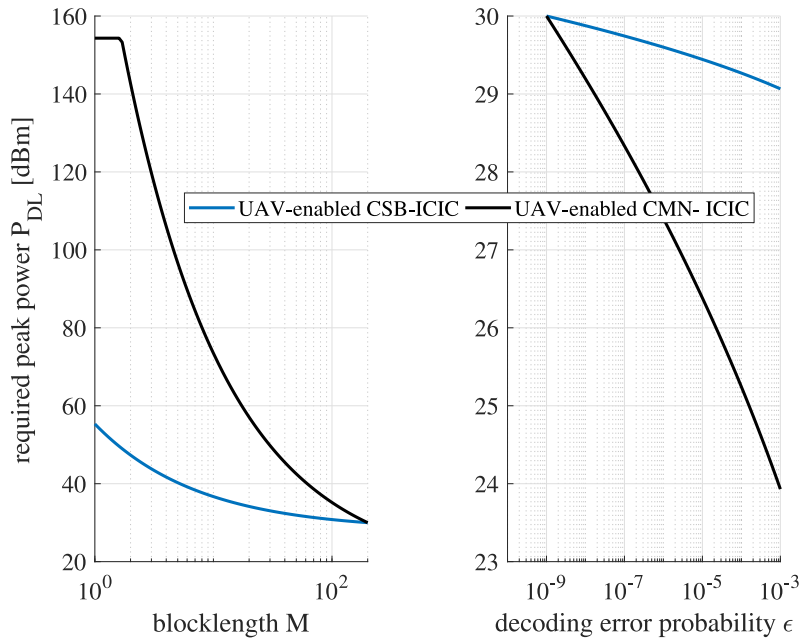

FIGURE 11. BS required peak transmit power versus blocklength and decoding error probability in the downlink.

performance, which is noticeable for blocklengths of around 200 symbols and a decoding error probability of 10^{-9}. Thus, the recommended scheme, which provides the best results for URLLC systems, requires moderately higher memory resources at the UAV as described earlier.

B. RESULTS FOR MULTI-UAV INTERFERENCE CASE

In Fig. 10, we consider sum achievable downlink data rates averaged over deployed UAVs, we compute $\bar{R}_{dl} = \frac{1}{N_{UAV}} \sum_k R_{T\ dl}(k)$, and then averaged it over all simulations,

and compare it to peak downlink power P_{dl}. Here, we observe that the conventional ICIC gives the worst results and the perfect UAV-assisted ICIC gives the best results. Furthermore, we see that the average data rate among deployed UAVs gets worse as the number of UAV N_{UAV} grows, which is intuitively expected, as the UAV have to share more of the same RB and hence the probability of interference is greater. In Fig. 4, we again consider BS peak downlink transmit power versus UAV sum achievable downlink rate, but we make a different comparison. First, one of the lines depending on

N_{UAV} and type of ICIC, from Fig. 10 is placed on each of the 4 subplots. This is always the middle line in each subplot which is colored orange. Moreover, around it, we average and maximize the maximums and similarly minimize the minimums in the following way. In each simulation, besides the average data rate, we also record the deviations of the minimum and maximum inter-UAV rates: $\min_k R_{T\ \text{dl}}(k) - \bar{R}_{\text{dl}}$ and $\max_k R_{T\ \text{dl}}(k) - \bar{R}_{\text{dl}}$. Then, we average these deviations and inter-UAV averages denoted $\bar{R}_{\text{dl}}$ over all simulations, subsequently, we add the simulation-averaged deviations back into the simulation-averaged inter-UAV averages. The extra steps help dampen the effect of variance between simulations due to the random nature of their initialization and ensure that deviation comparisons happen on a per-simulation basis. The resulting curves are adjacent to the middle curve in each subplot which is shown by red and purple lines. Additionally, aside from averaging the deviations over simulations, we also find the minimum of the down–deviations and maximum over the up-deviations over the simulations, adding them back into simulation-averaged $\bar{R}_{\text{dl}}$. This results in the outermost curves on each subplot shown by blue and green lines. Moreover, this graph helps us assess the average dispersion between the highest-rate UAV and the lowest-rate UAV. As we see, in the conventional ICIC we inevitably end up with some UAV having a 0 data rate, while with the perfect ICIC this was always avoided. This was done at the cost of reducing data rates of the top-performing UAV, as the top line is closer to the middle line in the perfect ICIC. Thus, we guarantee fairness among UAV for downlink communications. In the graphs that follow we explore the uplink. In Fig. 5, we observe the inter-simulation average of the inter-UAV average maximum interference power over the RBs assigned to the UAVs relative to threshold Γ_U. Here, we have set $P_{\text{ul}} = 10$ dBm and $M_u = 10$. Moreover, the interference for predicted CSI is computed with power allocation from (7), while interference for perfect CSI is computed with power allocation from (9). Now, we see that the perfect CSI does not perfectly follow a linear curve, which is not surprising. As the UAVs become operational one after the other, so each new UAV mitigates the interference it provides to BS without knowing which new RBs, the BSs will be assigned in the uplink for the UAVs that become operational afterward. Therefore, the dashed lines are for the most part above the identity line up to the plateau caused by the fact that power control is limited from above by peak power P_{ul}. Furthermore, the interference with predicted CSI denoted by solid lines is as expected, lower for each corresponding N_{UAV}. Also, despite the uneven nature of the lines, they are still, as should be, monotonously increasing up to the plateau. This is because a higher threshold allows for higher uplink power, which increases interference at the BSs. The effect from the variability of simulations is smoothed over by averaging over them, as is done in all graphs. Lastly, in Fig. 7, we plot how the sum uplink rate and maximum interference vary with each other by varying thresholds to obtain these values. Since for the conventional ICIC, there are no thresholds to vary, there is only one point for it on the

plot for each scenario. As with downlink, a higher number of UAVs generally worsens the data rate for a fixed interference, as does a lower number of RB candidates.

V. CONCLUSION

In this paper, we studied ICIC for the single and multi-UAV framework to facilitate URLLC services under perfect/imperfect CSI using cognitive radio. The goal was to mitigate strong ICI in such single and multi-UAV-assisted cellular networks. To achieve this goal, we modelled BS-to-UAV (B2U) interference in downlink communication, whereas in the uplink we modelled UAV-to-BS (U2B), UAV-to-UAV (U2U) and UE-to-UAV (UE2U), respectively. In this regard, we proposed low-complexity algorithms namely perfect ICIC, UAV-sensing assisted ICIC and perfect ICIC. Results showed that the proposed perfect ICIC provided fairness among UAVs especially in downlink communications compared to conventional ICIC algorithms. Lastly, we demonstrated in general, that the proposed UAV-sensing assisted ICIC and perfect ICIC algorithms gave better performance than conventional ICIC for both uplink and downlink for the single and multi-UAV framework.

REFERENCES

[1] U. M. Malik, M. A. Javed, S. Zeadally, and S. U. Islam, "Energy-efficient fog computing for 6G-enabled massive IoT: Recent trends and future opportunities," *IEEE Internet Things J.*, vol. 9, no. 16, pp. 14572–14594, Aug. 2022.

[2] Y. Liu, F. Han, and S. Zhao, "Flexible and reliable multiuser SWIPT IoT network enhanced by UAV-mounted intelligent reflecting surface," *IEEE Trans. Rel.*, vol. 71, no. 2, pp. 1092–1103, Jun. 2022.

[3] R. F. Hayat, S. Aurangzeb, M. Aleem, G. Srivastava, and J. C.-W. Lin, "ML-DDoS: A blockchain-based multilevel DDoS mitigation mechanism for IoT environments," *IEEE Trans. Eng. Manag.*, early access, May 13, 2022, doi: 10.1109/TEM.2022.3170519.

[4] Y. Yang et al., "ASTREAM: Data-stream-driven scalable anomaly detection with accuracy guarantee in IIoT environment," *IEEE Trans. Netw. Sci. Eng.*, early access, Mar. 8, 2022, doi: 10.1109/TNSE.2022.3157730.

[5] M. Bennis, M. Debbah, and H. V. Poor, "Ultrareliable and low-latency wireless communication: Tail, risk, and scale," *Proc. IEEE*, vol. 106, no. 10, pp. 1834–1853, Oct. 2018.

[6] G. Geraci et al., "What will the future of UAV cellular communications be? A flight from 5G to 6G," *IEEE Commun. Surveys Tuts.*, vol. 24, no. 3, pp. 1304–1335, 3rd Quart., 2022.

[7] U. Ahmed, J. C.-W. Lin, and G. Srivastava, "Deep fuzzy contrast-set deviation point representation and trajectory detection," *IEEE Trans. Fuzzy Syst.*, early access, Aug. 10, 2022, doi: 10.1109/TFUZZ.2022.3197876.

[8] M. A. Javed, T. N. Nguyen, J. Mirza, J. Ahmed, and B. Ali, "Reliable communications for cybertwin-driven 6G IoVs using intelligent reflecting surfaces," *IEEE Trans. Ind. Informat.*, vol. 18, no. 11, pp. 7454–7462, Nov. 2022.

[9] M. A. Javed and S. Zeadally, "AI-empowered content caching in vehicular edge computing: Opportunities and challenges," *IEEE Netw.*, vol. 35, no. 3, pp. 109–115, May/Jun. 2021.

[10] S. A. Moqurrab, A. Anjum, N. Tariq, and G. Srivastava, "Instant_anonymity: A lightweight semantic privacy guarantee for 5G-enabled IIoT," *IEEE Trans. Ind. Informat.*, vol. 19, no. 1, pp. 951–959, Jun. 2022.

[11] R. Gupta et al., "VAHAK: A blockchain-based outdoor delivery scheme using UAV for healthcare 4.0 services," in *Proc. IEEE Conf. Comput. Commun. Workshops (INFOCOM WKSHPS)*, 2020, pp. 255–260.

[12] R. Gupta, A. Nair, S. Tanwar, and N. Kumar, "Blockchain-assisted secure UAV communication in 6G environment: Architecture, opportunities, and challenges," *IET Commun.*, vol. 15, no. 10, pp. 1352–1367, 2021.

[13] Y. Liu, X. Ma, L. Shu, G. P. Hancke, and A. M. Abu-Mahfouz, "From industry 4.0 to agriculture 4.0: Current status, enabling technologies, and research challenges," *IEEE Trans. Ind. Informat.*, vol. 17, no. 6, pp. 4322–4334, Jun. 2021.

[14] C. She et al., "A tutorial on ultrareliable and low-latency communications in 6G: Integrating domain knowledge into deep learning," *Proc. IEEE*, vol. 109, no. 3, pp. 204–246, Mar. 2021.

[15] W. Saad, M. Bennis, and M. Chen, "A vision of 6G wireless systems: Applications, trends, technologies, and open research problems," *IEEE Netw.*, vol. 34, no. 3, pp. 134–142, May/Jun. 2020.

[16] K. B. Letaief, W. Chen, Y. Shi, J. Zhang, and Y.-J. A. Zhang, "The roadmap to 6G: AI empowered wireless networks," *IEEE Commun. Mag.*, vol. 57, no. 8, pp. 84–90, Aug. 2019.

[17] L. Bariah et al., "A prospective look: Key enabling technologies, applications and open research topics in 6G networks," *IEEE Access*, vol. 8, pp. 174792–174820, 2020.

[18] D. Maaz, A. Galindo-Serrano, and S. E. Elayoubi, "URLLC user plane latency performance in new radio," in *Proc. IEEE 25th Int. Conf. Telecommun.*, 2018, pp. 225–229.

[19] Y. Polyanskiy, H. V. Poor, and S. Verdú, "Channel coding rate in the finite blocklength regime," *IEEE Trans. Inf. Theory*, vol. 56, no. 5, pp. 2307–2359, May 2010.

[20] A. Fotouhi et al., "Survey on UAV cellular communications: Practical aspects, standardization advancements, regulation, and security challenges," *IEEE Commun. Surveys Tuts.*, vol. 21, no. 4, pp. 3417–3442, 4th Quart., 2019.

[21] Y. Guo, S. Yin, J. Hao, and Y. Du, "A novel trajectory design approach for UAV based on finite Fourier series," *IEEE Wireless Commun. Lett.*, vol. 9, no. 5, pp. 671–674, May 2020.

[22] K. Wang, C. Pan, H. Ren, W. Xu, L. Zhang, and A. Nallanathan, "Packet error probability and effective throughput for ultra-reliable and low-latency UAV communications," *IEEE Trans. Commun.*, vol. 69, no. 1, pp. 73–84, Jan. 2021.

[23] J. Lyu, Y. Zeng, and R. Zhang, "Cyclical multiple access in UAV-aided communications: A throughput-delay tradeoff," *IEEE Wireless Commun. Lett.*, vol. 5, no. 6, pp. 600–603, Dec. 2016.

[24] S. Ahmed, M. Z. Chowdhury, and Y. M. Jang, "Energy-efficient UAV relaying communications to serve ground nodes," *IEEE Commun. Lett.*, vol. 24, no. 4, pp. 849–852, Apr. 2020.

[25] A. Ranjha and G. Kaddoum, "URLLC-enabled by laser powered UAV relay: A quasi-optimal design of resource allocation, trajectory planning and energy harvesting," *IEEE Trans. Veh. Technol.*, vol. 71, no. 1, pp. 753–765, Jan. 2022.

[26] A. Ranjha, G. Kaddoum, and K. Dev, "Facilitating URLLC in UAV-assisted relay systems with multiple-mobile robots for 6G networks: A prospective of agriculture 4.0," *IEEE Trans. Ind. Informat.*, vol. 18, no. 7, pp. 4954–4965, Jul. 2022.

[27] A. Ranjha, G. Kaddoum, M. Rahim, and K. Dev, "URLLC in UAV-enabled multicasting systems: A dual time and energy minimization problem using UAV speed, altitude and beamwidth," *Comput. Commun.*, vol. 187, pp. 125–133, Apr. 2022.

[28] J. M. Meredith, "Study on enhanced LTE support for aerial vehicles," 3GPP, Sophia Antipolis, France, Rep. 36.777, 2017.

[29] X. Lin et al., "The sky is not the limit: LTE for unmanned aerial vehicles," *IEEE Commun. Mag.*, vol. 56, no. 4, pp. 204–210, Apr. 2018.

[30] X. Li and J. Xu, "Positioning optimization for sum-rate maximization in UAV-enabled interference channel," *IEEE Signal Process. Lett.*, vol. 26, no. 10, pp. 1466–1470, Oct. 2019.

[31] W. Mei and R. Zhang, "UAV-sensing-assisted cellular interference coordination: A cognitive radio approach," *IEEE Wireless Commun. Lett.*, vol. 9, no. 6, pp. 799–803, Jun. 2020.

[32] H. Ren, C. Pan, K. Wang, Y. Deng, M. Elkashlan, and A. Nallanathan, "Achievable data rate for URLLC-enabled UAV systems with 3-D channel model," *IEEE Wireless Commun. Lett.*, vol. 8, no. 6, pp. 1587–1590, Dec. 2019.

ALI RANJHA received the bachelor's degree in electrical engineering from the Comsats Institute of Information Technology, Lahore, Pakistan, in 2014, the M.S. degree in telecommunications from Lancaster University, U.K., in 2018, and the Ph.D. degree in facilitating URLLC in UAV networks for 5G and beyond systems from the École de Technologie Supérieure Université du Québec, Montréal, Canada, in 2022. His research interests span diverse areas, such as fundamental communication theory, unmanned aerial vehicle communications, Internet of Things, ultra-reliable and low latency communications, and optimization in resource-constrained networks.

MUHAMMAD AWAIS JAVED received the B.Sc. degree in electrical engineering from the University of Engineering and Technology Lahore, Pakistan, in August 2008, and the Ph.D. degree in electrical engineering from the University of Newcastle, Australia, in February 2015. From July 2015 to June 2016, he was a Postdoctoral Research Scientist with the Qatar Mobility Innovations Center on SafeITS Project. He is currently working as an Associate Professor with COMSATS University Islamabad, Pakistan. His research interests include intelligent transport systems, vehicular networks, protocol design for emerging wireless technologies, and the Internet of Things.

GAUTAM SRIVASTAVA (Senior Member, IEEE) is an Associate Professor with Brandon University, Manitoba, Canada.. He has authored or coauthored a total of 400 papers in conferences or high-status journals and has also delivered invited guest lectures on big data, cloud computing, the Internet of Things, and cryptography. His research is funded by federal grants from the Natural Sciences and Engineering Research Council of Canada and MITACS. His research interests include data mining, big data, and IoT.

JERRY CHUN-WEI LIN (Senior Member, IEEE) received the Ph.D. degree in computer science and information engineering, National Cheng Kung University, Tainan, Taiwan, in 2010. He is a Professor with the Western Norway University of Applied Sciences, Bergen, Norway. He has published more than 500 research papers in peer-reviewed international conferences and journals. His research interests include data mining, big data analytics, and social network. He is the Editor-in-Chief of the *Data Science and Pattern Recognition* and an Associate Editor of several top-tier journals including IEEE TRANSACTIONS ON NEURAL NETWORKS AND LEARNING SYSTEMS, IEEE TRANSACTIONS ON CYBERNETICS, and IEEE TRANSACTIONS ON DEPENDABLE AND SECURE COMPUTING. He is a Senior ACM Distinguisehd Scientist and a Fellow of IET.